Annals of Nuclear Energy 120 (2018) 798–804

Contents lists available at ScienceDirect

Annals of Nuclear Energy

journal homepage: www.elsevier.com/locate/anucene

# Effects of ballooning and rupture on the fracture resistance of Zircaloy-4 fuel cladding tube after LOCA-simulated experiments

Takanori Yumura, Masaki Amaya *

*Nuclear Safety Research Center, Japan Atomic Energy Agency, 2-4, Shirakata, Tokai-mura, Naka-gun, Ibaraki 319-1195, Japan*

ARTICLE INFO

*Article history:*
Received 25 May 2018
Received in revised form 22 June 2018
Accepted 26 June 2018
Available online 19 July 2018

*Keywords:*
Zircaloy-4
LOCA
Fuel cladding
Ballooning
Rupture
Four-point bending test
Oxidation
Prior-β layer

ABSTRACT

To investigate the relationship between the fracture resistance of a cladding tube and the amount of deformation of the cladding tube due to ballooning and rupture during a loss-of-coolant accident (LOCA), four-point-bending tests were performed using non-irradiated Zircaloy-4 cladding tubes which experienced a LOCA-simulated sequence (ballooning, rupture, high temperature oxidation and quench). According to the obtained results, it was found that the maximum bending stress of the cladding tube after the LOCA-simulated sequence, which was defined as the fracture resistance, correlated to the average thickness of prior-β layer in the cladding tube. Based on the average thickness of prior-β layer, the fracture resistance of the cladding tube with ballooning and rupture was expressed as functions of isothermal oxidation time and temperature and the maximum circumferential strain on the cladding tube.



## 1. Introduction

During a large-break loss-of-coolant accident (LB-LOCA) in a light water reactor, fuel cladding would experience deformation and embrittlement caused by the oxidation and hydrogen absorption at high temperature in a steam atmosphere. After the emergency core cooling system (ECCS) is activated and cooling water is injected into the reactor core, a tensile load would be applied to the fuel cladding by the restraint between fuel cladding and spacer and thermal shock (Chung et al., 1980). Current Japanese LOCA criteria are determined to maintain the coolability of the reactor core during and after a LOCA by avoiding the embrittlement of fuel cladding by oxidation and secondary hydriding. The criteria require that the peak cladding temperature (PCT) shall not exceed 1200 °C (1473 K) and the amount of oxidation, which is expressed as an equivalent cladding reacted (ECR) calculated by the Baker-Just oxidation equation (Baker and Just, 1962), shall not exceed 15%. The appropriateness of these criteria has been investigated and verified by previous studies (Uetsuka et al., 1983; Nagase and Fuketa, 2004; Nagase et al., 2009; Uetsuka et al., 1981).

Maintaining fuel rod shape during the long-term core cooling after LOCA has become a key issue related to nuclear safety since the accident at the Fukushima Daiichi nuclear power station. Especially, an earthquake is considered as one of the major external forces which would apply a load to the fuel rod in the reactor core during the long-term core cooling, and it is important to evaluate the fracture resistance of fuel rods against such seismic load in order to estimate the long-term core coolability after LOCA. While effects of the oxidation and hydrogen embrittlement for the fracture resistance have been investigated by preceding studies (Yamato et al., 2014; Billone et al., 2016) by four-point bending test (4PBT), which simulates an external force caused by seismic motion, effects of deformation of the fuel cladding due to ballooning and rupture during LOCA on the fracture resistance of fuel cladding have not been clarified yet.

In this study, the relationship between the fracture resistance of the cladding tube and the deformation of the cladding tube due to ballooning and rupture during a LOCA was investigated by 4PBT using non-irradiated Zircaloy-4 cladding tubes which experienced a LOCA-simulated sequence; and was formulated as functions of the isothermal oxidation temperature and time and the maximum circumferential strain on the cladding tube.

## 2. Experimental

### 2.1. Test specimen and apparatus

Fig. 1 shows a schematic diagram of a test rod used in this study. The test rod consisted of an un-irradiated stress-relieved

* Corresponding author.
*E-mail address:* amaya.masaki@jaea.go.jp (M. Amaya).

https://doi.org/10.1016/j.anucene.2018.06.046
0306-4549/

**Nomenclature**

| | |
|---|---|
| $L'$ | outside circumferential length after ballooning and burst [m] |
| $r_1$ | inner radius as received [m] |
| $r_2$ | outer radius as received [m] |
| $r'_1$ | inner radius after ballooning and burst [m] |
| $r'_2$ | outer radius after ballooning and burst [m] |
| $r''_1$ | inner radius after oxidation and quench [m] |
| $r''_2$ | outer radius after oxidation and quench [m] |
| $\delta_{nom}$ | wall thickness as received [m] |
| $\delta'$ | wall thickness of maximum circumferential strain [m] |
| $\delta'_r$ | wall thickness of the Zircaloy-4 metal layer reacted with steam which corresponds to a target ECR [m] |
| $\delta_{prior-\beta}$ | average thickness of prior-β layer defined as Eq. (9) [m] |
| $\delta_{\alpha-Zr(O)}$ | average thickness of α-Zr(O) layer defined as Eq. (10) [m] |
| $\delta_{ZrO_2}$ | average thickness of $ZrO_2$ layer defined as Eq. (11) [m] |
| $\delta^E_{prior-\beta}$ | average thickness of prior-β layer evaluated by using Eq. (16) [$\times 10^{-6}$m] |
| $\delta^E_{\alpha-Zr(O)}$ | average thickness of α-Zr(O) layer evaluated by using Eq. (15) [m] |
| $\delta^E_{ZrO_2}$ | average thickness of $ZrO_2$ layer evaluated by using Eq. (14) [m] |
| $ECR_{Target}$ | target ECR for the experiment [%] |
| $t$ | isothermal oxidation time [s] |
| $g_{Zr}$ | density of Zr (6500[kg/m$^3$]) (Baker and Just, 1962) |
| $R_{B-J}$ | gas constant used in the Baker-Just oxidation equation (1.987 [cal/mol-K]) (Baker and Just, 1962) |
| $R$ | gas constant (8.31451 [J/mol-k]) |
| $T$ | isothermal oxidation temperature [K] |
| $\sigma^M_{bending}$ | maximum bending stress during 4PBT [MPa] |
| $\sigma^E_{bending}$ | maximum bending stress evaluated by Eq. (13) [MPa] |
| $M$ | maximum bending moment [N-m] |
| $P_{max}$ | maximum load [N] |
| $\theta$ | rupture opening angle which is evaluated using the width of the rupture opening and the outer radius [rad] |
| $l_1$ | span between loading pins [m] |
| $l_2$ | span between support pins [m] |
| $A_{prior-\beta}$ | area of prior-β layer [m$^2$] |
| $A_{prior-\beta+\alpha-Zr(O)}$ | total area of α-Zr(O) and prior-β layers[m$^2$] |
| $A_{prior-\beta+\alpha-Zr(O)+ZrO_2}$ | total area of $ZrO_2$, α-Zr(O) and prior-β layers [m$^2$] |
| $CL_{prior-\beta}$ | circumferential length of the central line in the cladding wall after oxidation between the outer edges of prior-β layer [m] |
| $CL_{prior-\beta+\alpha-Zr(O)}$ | circumferential length of the central line in the cladding wall after oxidation between the outer edges of α-Zr(O) layer (including prior-β layer) [m] |
| $CL_{prior-\beta+\alpha-Zr(O)+ZrO_2}$ | circumferential length of the central line in the cladding wall after oxidation between the outer edges of $ZrO_2$ layer (including α-Zr(O) and prior-β layers) [m] |
| $C_m$ | maximum circumferential strain [%] |

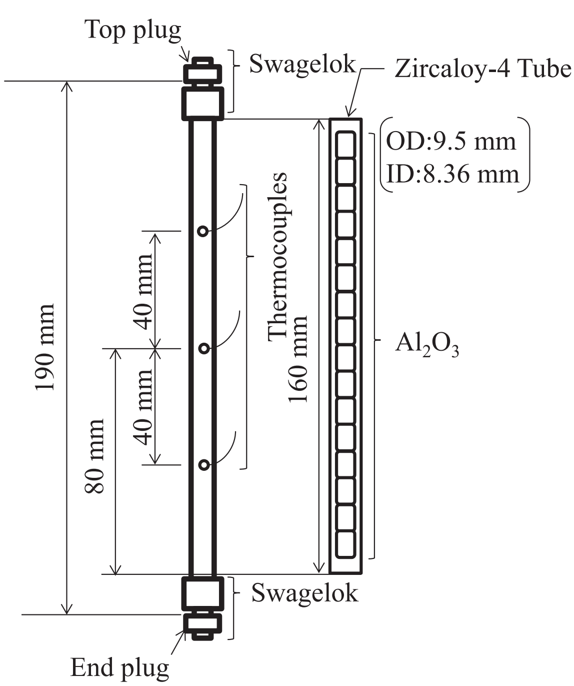


**Fig. 1.** A schematic diagram of the test rod used in this study.

Zircaloy-4 cladding tube, alumina pellets and end plugs. The length, outer diameter and wall thickness of the tube were approximately 190, 9.5, and 0.57 mm, respectively. Here, alumina pellets were used to simulate the effect of the heat capacity of $UO_2$ on the temperature change in the cladding during a LOCA. After alumina pellets were inserted into the cladding tube, the end plugs were connected to the upper and lower ends of the cladding tube using Swagelok™. Three R-type thermocouples were spot-welded on the outer surface of the cladding tube: the axial positions were the center of specimen, 40 mm above and below the center of the test fuel rod, respectively.

A schematic diagram of the test apparatus is presented in Fig. 2. The test apparatus consists of a tensile-testing-machine with a

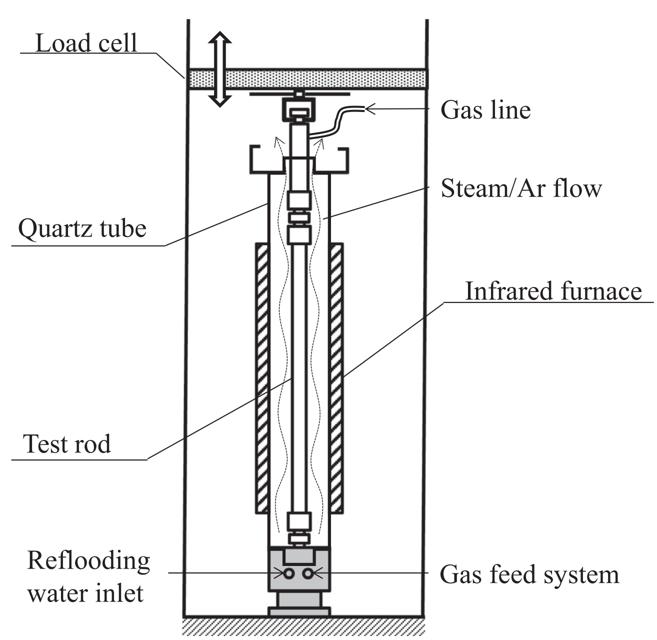


**Fig. 2.** A schematic diagram of the test apparatus used in this study.